Supporting Information

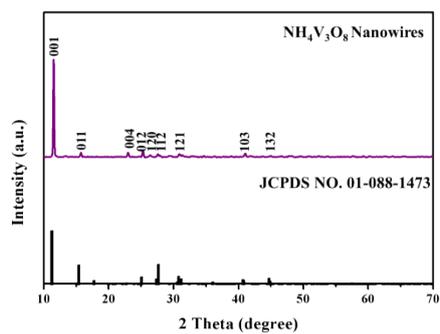
Figure S1. XRD pattern of $NH_4V_3O_8$ nanowires.
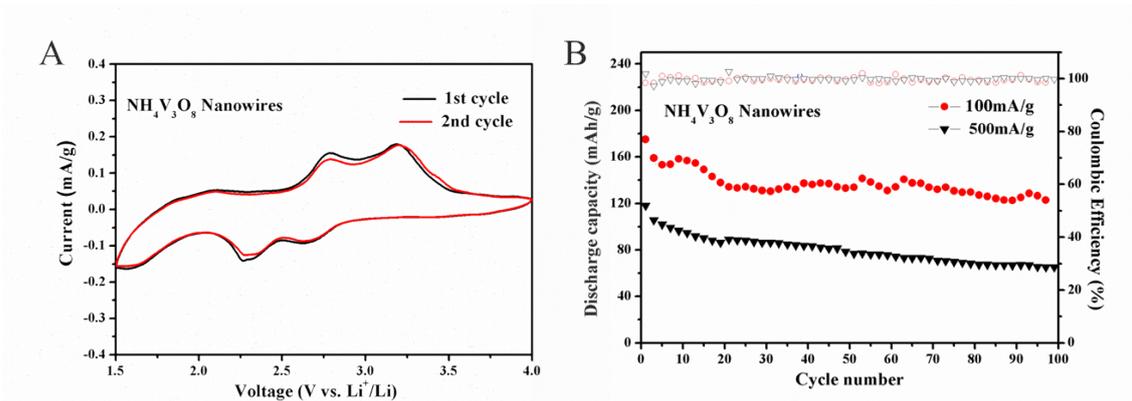
Figure S2.CV curves (a) and cycle performance (b) of NH$_4$VO$_8$ nanowires.
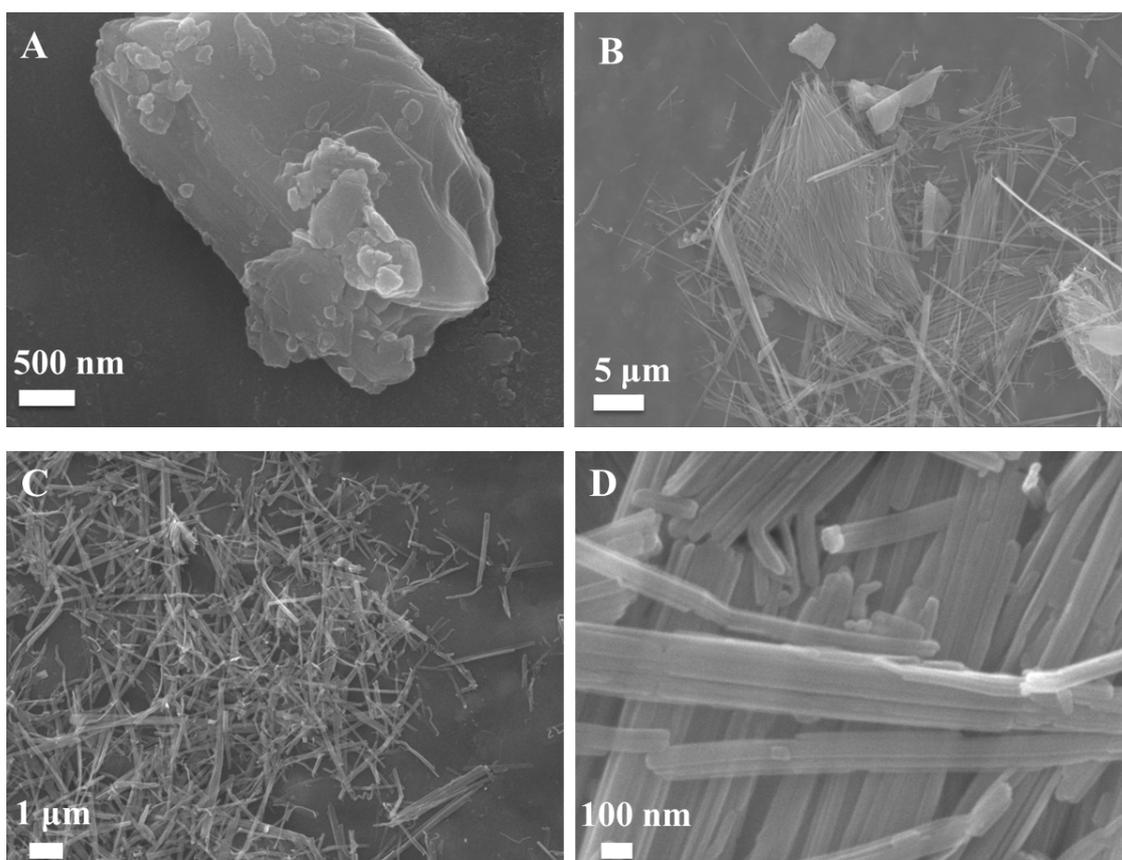
Figure S3. SEM images of $NH_4V_3O_8$ obtained in different condition: hydrothermal time is 3 days (A); 5 days (B); 7 days (C, D).

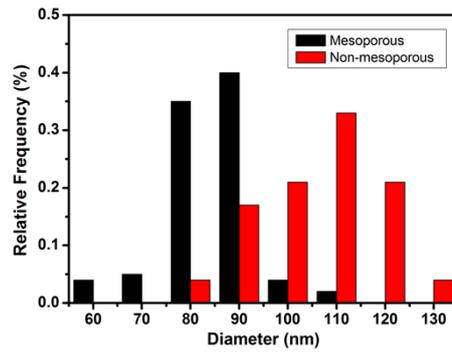Figure S4. Statistical analysis of diameters of $NH_4V_3O_8$ nanowires (black) and mesoporous VO_2 nanowires (red).
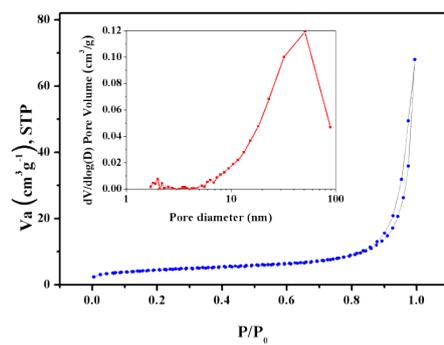
Figure S5. Desorption isotherms and pore size distribution (inset) of $NH_4V_3O_8$ nanowires.
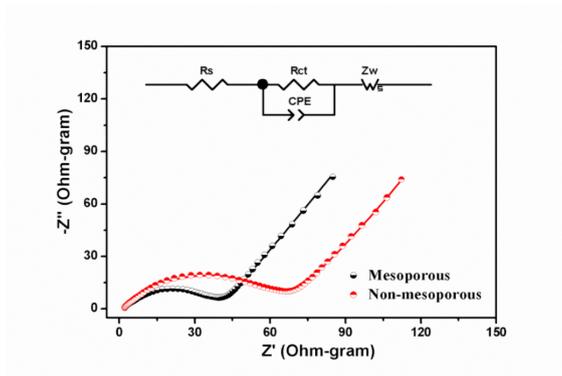
Figure S6. Variations and fittings between Z_{re} and the reciprocal square root of the angular frequency in the low frequency region of mesoporous (black) and non-mesoporous (red) VO_2 nanowires.
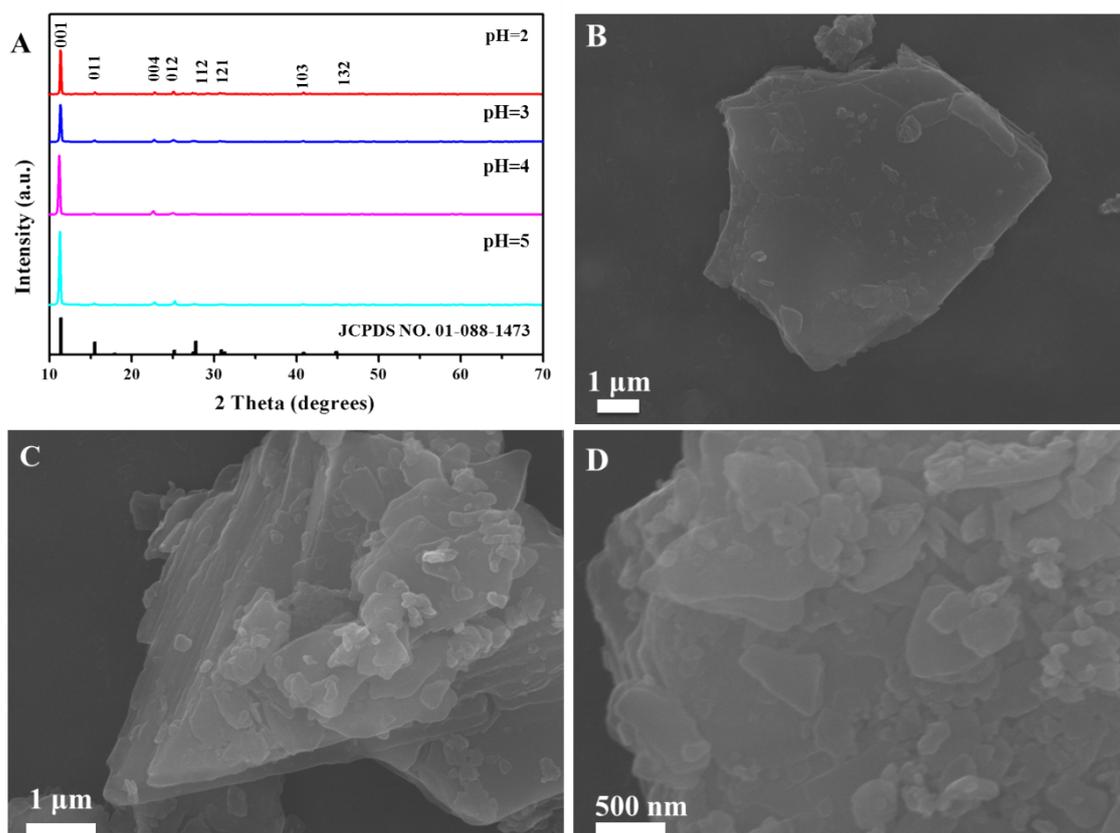
Figure S7. XRD pattern of obtained $NH_4V_3O_8$ in different condition: pH=2(red) pH=3 (blue); pH=4 (purple); pH=5 (light blue). SEM images of NH4V3O8 obtained in different condition: pH=3 (B); pH=4 (C); pH=5 (D).
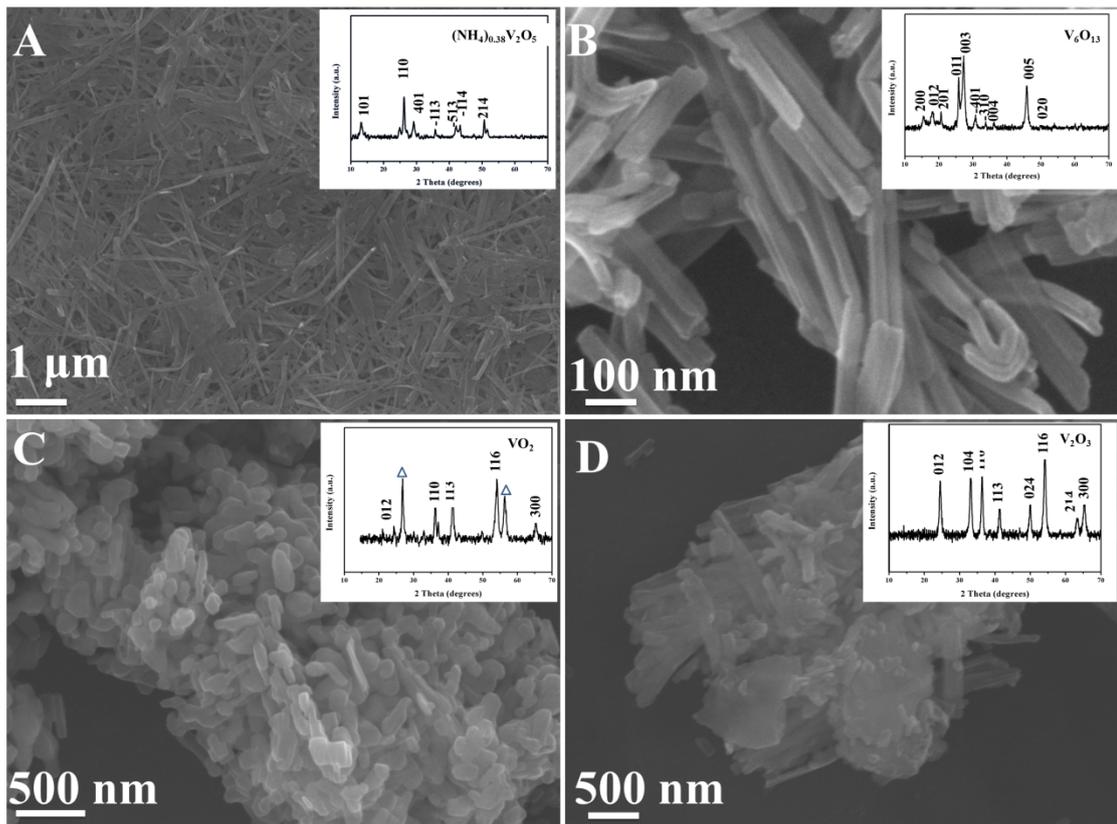
Figure S8. SEM images (inset is the corresponding XRD pattern) of obtained products in different annealing condition: 300°C (A); 350°C (B); 450°C (C); 500°C (D).
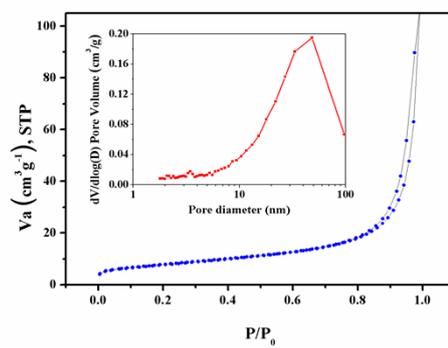
Figure S9. Desorption isotherms and pore size distribution (inset) of $(NH_4)_{0.38}V_2O_5$ nanowires obtained at the annealing temperature of 350°C.
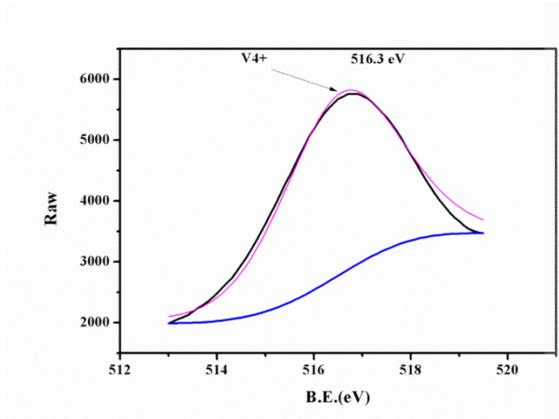
Figure S10. XPS spectrum of mesoporous VO$_2$ nanowires.